Ecotoxicology and Environmental Safety 273 (2024) 116179

Contents lists available at ScienceDirect

Ecotoxicology and Environmental Safety

journal homepage: www.elsevier.com/locate/ecoenv

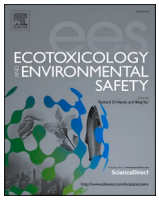

Evidence for chromium crosses blood brain barrier from the hypothalamus in chromium mice model

Jiuyang Ding [a,b,c,1], Baofei Sun [a,1], Yingdong Gao [d], Juan Zheng [d], Changyou Liu [e], Jian Huang [f], Nannan Jia [g], Xianglin Pei [h], Xueyu Jiang [i], Shanshan Hu [j], Bing Xia [c], Yunle Meng [k], Zhuihui Dai [l,*], Xiaolan Qi [b,**], Jiawen Wang [c,***]

[a] Key Laboratory of Human Brain bank for Functions and Diseases of Department of Education of Guizhou Province, Guizhou Medical University, Guiyang 550025, China
[b] Key Laboratory of Endemic and Ethnic Diseases, Ministry of Education, Guizhou Medical University, Guiyang 550004, China
[c] School of Forensic Medicine, Guizhou Medical University, Guiyang 550004, China
[d] Department of Reproductive Medicine, Taian Maternity and Child Health Hospital, Taian 271000, China
[e] Department of Pediatrics, Taian Maternity and Child Health Hospital, Taian 271000, China
[f] School of Forensic Medicine, Kunming Medical University, Kunming 650500, China
[g] Neonatal Screening Center, Taian Maternity and Child Health Hospital, Taian, China
[h] School of Materials and Architectural Engineering, Guizhou Normal University, Guiyang 550025, China
[i] College of Food Science and Engineering, Wuhan Polytechnic University, Wuhan 430023, China
[j] Good Clinical Practice Center, Affiliated Hospital of Zunyi Medical University, Zunyi 563003, China
[k] Institute of Forensic Science, Ministry of Public Security, Beijing 100038, China
[l] State Key Laboratory of Ore Deposit Geochemistry, Institute of Geochemistry, Chinese Academy of Sciences, Guiyang 550081, China

ARTICLE INFO

Edited by Dr Yong Liang

Keywords:
Chromium
Blood brain barrier
Hypothalamus

ABSTRACT

It has been shown that exposure to hexavalent Chromium, Cr (VI), via nasal cavity can have neurotoxicological effects and induces behavioral impairment due to the fact that blood brain barrier (BBB) does not cover olfactory bulb. But whether Cr (VI) can cross the BBB and have a toxicological effects in central nervous system (CNS) remains unclear. Therefore, we investigated the effects of Cr (VI) on mice treated with different concentrations and exposure time (14 days and 28 days) of Cr (VI) via intraperitoneal injection. Results revealed that Cr accumulated in hypothalamus (HY) in a timely dependent manner. Much more severer neuropathologies was observed in the group of mice exposed to Cr (VI) for 28 days than that for 14 days. Gliosis, neuronal morphological abnormalities, synaptic degeneration, BBB disruption and neuronal number loss were observed in HY. In terms of mechanism, the Nrf2 related antioxidant stress signaling dysfunction and activated NF-κB related inflammatory pathway were observed in HY of Cr (VI) intoxication mice. And these neuropathologies and signaling defects appeared in a timely dependent manner. Taking together, we proved that Cr (VI) can enter HY due to weaker BBB in HY and HY is the most vulnerable CNS region to Cr (VI) exposure. The concentration of Cr in HY increased along with time. The accumulated Cr in HY can cause BBB disruption, neuronal morphological abnormalities, synaptic degeneration and gliosis through Nrf2 and NF-κB signaling pathway. This finding improves our understanding of the neurological dysfunctions observed in individuals who have occupational exposure to Cr (VI), and provided potential therapeutic targets to treat neurotoxicological pathologies induced by Cr (VI).

* Corresponding author at: State Key Laboratory of Environmental Geochemistry, Institute of Geochemistry, Chinese Academy of Sciences, West Lincheng road, Guanshanhu district, Guiyang 550081, China.
** Corresponding author at: Key Laboratory of Endemic and Ethnic Diseases, Ministry of Education, Guizhou Medical University, No. 9 Beijing Road, Yunyan District, Guiyang, Guizhou 550004, China.
*** Corresponding author at: Department of Forensic Medicine, Guizhou Medical University, No. 9 Beijing Road, Yunyan District, Guiyang, Guizhou 550004, China.
E-mail addresses: daizhihui@mail.gyig.ac.cn (Z. Dai), xlq@gmc.edu.cn (X. Qi), wjwwfs@126.com (J. Wang).
[1] These authors contributed equally to this work.

https://doi.org/10.1016/j.ecoenv.2024.116179
Received 26 December 2023; Received in revised form 27 February 2024; Accepted 3 March 2024
Available online 8 March 2024

1. Introduction

Chromium (Cr), first discovered in 1797, is one of the top ten abundant elements on earth (Holmes et al., 2008). Cr mainly exists in two prevalent forms, trivalent chromium [Cr (III)] and hexavalent [Cr (VI)]. The Cr (III) is generally considered as nontoxic form but Cr (VI) due to its high toxic effect, has been listed as an environmental pollutant (DesMarais and Costa, 2019; Huang et al., 2022, 2021). Cr (VI) has been regarded as a heavy metal pollutant in 1998 and has gained much attention in recent years (Huang et al., 2018, 2020; Shaw et al., 2020). Industrial exposure or drinking water induced Cr (VI) toxicity have also drawn much attention in recent years (Wise et al., 2022).

Cr (VI) has been shown to account for several types of cancers (Qie et al., 2022). Recent studies find Cr (VI) is also neurotoxic (Salama and Elgohary, 2021). Cr (VI) in the air could be absorbed by olfactory bulb and be transferred into the brain due to lack of blood brain barrier (BBB) in the olfactory bulb (Hanson and Frey, 2008). Several animal model studies observed neurotoxicity by potassium dichromate through intraperitoneal injection (Doker et al., 2010). However, whether Cr (VI) could enter CNS across the BBB is still in debate. Many studies differentially showed that the highest level of Cr was in pituitary, hypothalamus (HY), cerebellum (CB) or temporal lobe in human brain (Calderon-Garciduenas et al., 2013; Civit et al., 2000; Rajan et al., 1997). However, the spatial deposition of Cr in the brain has not been elucidated clearly. Identifying the distribution of Cr in the brain should help to understand whether Cr could enter the brain and the pathway for Cr to enter the brain.

The BBB, consisted of astrocyte end feet, pericytes and endothelial cells, is a biological barrier to maintain the brain microenvironment (Kim et al., 2013; Reale et al., 2023). HY, as part of the hypothalamus - pituitary - adrenal gland (HPA) axis, produces neuroendocrine hormones that need to cross the BBB into the vessels (Carrera-Gonzalez et al., 2022; Khamirchi et al., 2020). Thus the BBB in HY is weaker among the whole brain (Haddad-Tovolli et al., 2017). Based on this, we speculate that the Cr (VI) might be able to cross the BBB in HY and accumulate in the brain.

Following heavy metals load, the reactive oxygen species and neuroinflammatory cytokines are dramatically induced. Recent studies revealed glutathione, interleukin 1-beta (IL-1β) and astrocyte number were remarkably increased in rats following Cr (VI) intranasal administration (Hegazy et al., 2021). However, they only conducted astrocyte analysis in cortical area. Thus, understanding the morphology and number of glial cells in different brain regions is crucial for elucidating the regional specificity of Cr (VI) intoxication.

A recent study found that the intranasal exposure of Cr (VI) caused oxidative stress, neuropathologies, and behavioral abnormalities in a timely dependent manner, but the applied concentrations of Cr were not analyzed (Hegazy et al., 2021). Thus, we thought that the brain Cr level was dependent on dose and duration of exposure. Inspired by the above research work, we analyzed the temporal and spatial distribution of Cr in mice exposed intraperitoneally to $K_2Cr_2O_7$ and the neuropathologies were assessed. In our study, we set two exposure durations which are 14 days and 28 days respectively and a single dose of Cr (VI) was set at 6 mg/kg body weight (0.25 LD_{50}) according to (Wise et al., 2022). The Cr levels in each brain regions were measured using inductively coupled plasma (ICP). In addition, the histopathological alterations and glial activation were analyzed in vulnerable brain regions of Cr (VI) exposure. The specific proteins of oxidation reduction process were tested in the Cr accumulated brain areas. We revealed a crucial pathogenic role of Cr (VI) in HY neurodegeneration and the mechanisms involved. To the best of our knowledge, there are still no evidences about BBB penetration and brain distribution pattern of Cr (VI) in mouse models after intoxication.

Table 1
Certified and observed values (μg g^{-1}) of Cr in quality control materials.

CRM	Element	Certified value	MW digestion (Mean±SEM)	Recovery(%)
DOLT-5	Cr	2.35±0.58	2.29±0.61	95

2. Materials and methods

2.1. Animal and experimental scheme

All animal experiments were conducted in accordance with National Institutes of Health (NIH) guidance and were approved by the Guizhou Medical University Animal Care and Use Committee. C57BL/6 J mice (male 20~25 g, 6~8 weeks old) were purchased from Laboratory Animal Center of Guizhou Medical University and were housed in temperature controlled room. Animals were fed with standard food and water.

After 7 days of acclimatization, mice were randomly divided into 3 groups (n = 19 mice per group): (1) Con (Control group), saline was administered intraperitoneally to mice, in place of potassium dichromate soluation ($K_2Cr_2O_7$, CAS No. 7778–50–9, Aladdin Co., Ltd. Shanghai, China); (2) Cr 14 days (Chromium exposure for 14 days), potassium dichromate solution (6 mg/kg body weight, dissolved in saline at the concentration of 0.1 mg/mL) was administered intraperitoneally to mice once daily for 14 days; (3) Cr 28 days (Chromium exposure for 28 days), potassium dichromate solution (6 mg/kg body weight, dissolved in saline at the concentration of 0.1 mg/mL) was administered intraperitoneally to mice once daily for 28 days.

2.2. Inductively coupled plasma (ICP)

Mice were anesthetized with ketamine (120 mg/kg) and (xylazine 8 mg/kg) intraperitoneally. Then the mice were perfused with 100 mL saline from the left ventricle to flush out the blood in the brain. Whole fresh mice brain were obtained. Brain regions, including olfactory bulb (OB), prefrontal cortex (PFC), somatosensory cortex (Cortex), striatum (STR), hippocampus (Hippo), thalamus(TH), hypothalamus (HY), cerebellum (CB), midbrain (MB) and medulla were detached under a dissecting microscope (125 M, Leica, Germany). Microwave (MW) digestion techniques for organism samples were compared in this study. 20 mg of sample was dissolved in 6 mL of nitrohydrochloric acid, 2 mL of 30% H_2O_2 solution and 1 mL hydrofluoric acid solution. The mixture was placed in MW system. A program of 240 min was used during digestion procedure (120 min, 150 ^{0}C; 120 min, 210 ^{0}C). At the end of the procedure, the solutions were completed to a volume of 10 mL using ultradistilled water. Inductively Coupled Plasma Optical Emission Spectrometer (ICP-OES, Avio 200 Pekin-Elmer, Shelto, CT, USA) with 357.9 nm wavelength lines was used for the determination of concentration of chromium according to the protocol provided by the manufacturer. Performance of the method was evaluated in terms of linearity, recovery and precision. The data obtained for concentrations of Cr in Fish Protein Certified Reference Material (DOLT-5) were used to validate the method (Table 1) (Grochowski et al., 2019). The test method of CRM was same as brain samples. And five DOLT-5 samples were tested.

2.3. Hematoxylin and eosin (HE) staining and silver staining

Briefly, whole brain of mice were fixed in 4% paraformaldehyde (PFA) for 48 hrs. After dehydration and embedding in wax, brain samples were sectioned (3μm in thickness) and mounted on glass slides. For HE staining, sections were stained with hematoxylin for 1 min before rinsing in eosin for 1 min. For silver staining, brain sections were rinsed in acid formaldehyde for 3 min, and then in 0.25% silver nitrate solution at 37 ^{0}C for 2 min. After rinsing in gallic hydroxide, tissues were washed using tap water. All sections were sealed with neutral gum. Images were taken using a microscope (CX23, Olympus, Japan).

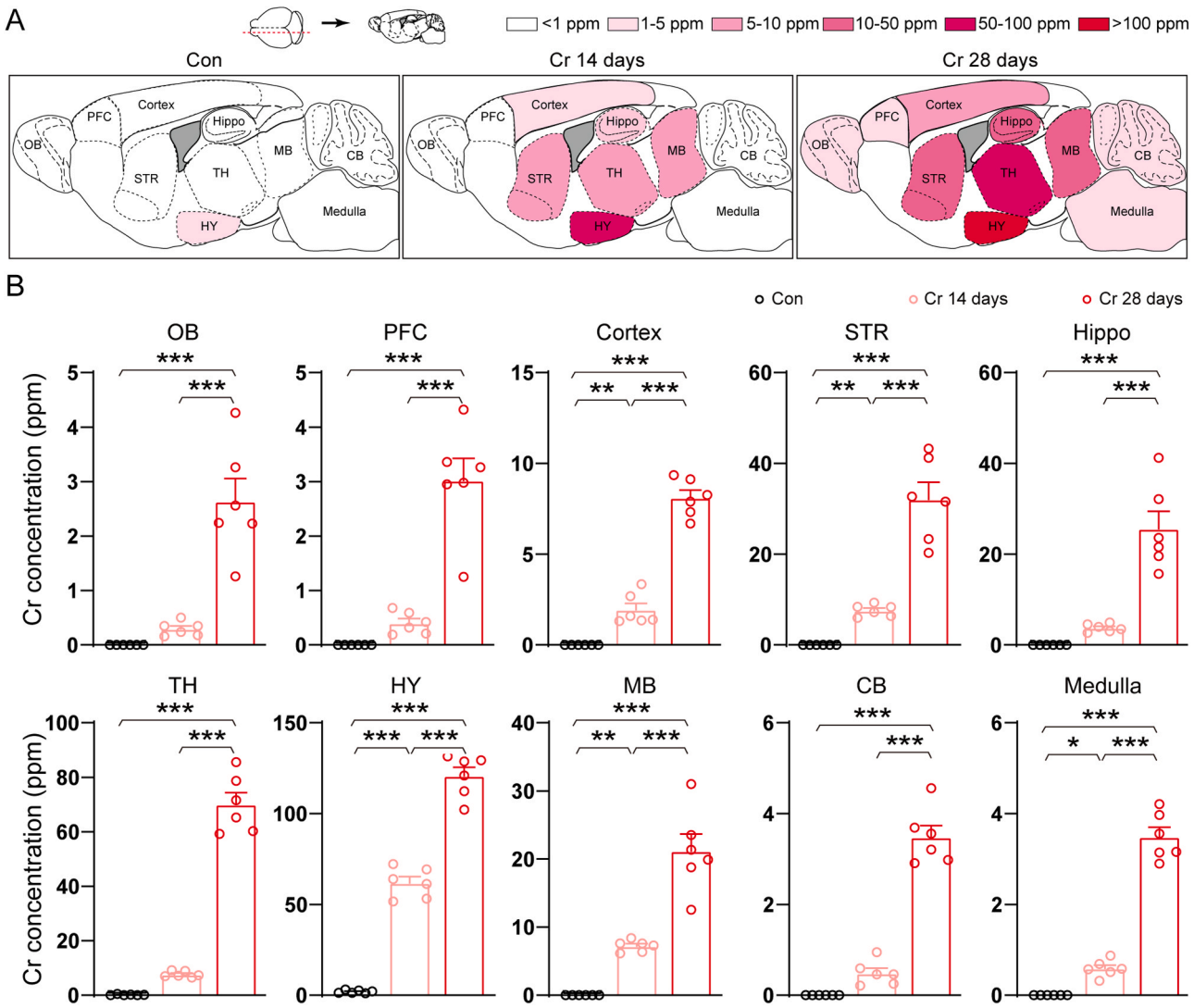

Fig. 1. The Cr accumulation level in different brain areas using ICP analysis. (A) Semiquantitative of Cr concentrations in brains from control, 14 days Cr exposure and 28 days Cr exposure mice. (B) Quantification of the Cr concentrations in different brain areas. OB: F (2, 17) = 35.175, $P < 0.001$, PFC: F (2, 17) = 46.514, $P < 0.001$, Cortex: F (2,17)= 178.805, $P < 0.001$, STR: F (2, 17) = 58.421, $P < 0.001$, Hippo: F (2, 17) = 38.648, $P < 0.001$, TH: F (2, 17) = 237.507, $P < 0.001$, HY: F (2, 17) = 311.477, $P < 0.001$, MB: F (2, 17) = 55.659, $P < 0.001$, CB: F (2, 17) = 144.154, $P < 0.001$, Medulla: F (2, 17) = 209.187, $P < 0.001$. n = 6 mice, $^{*}p < 0.05$, $^{**}p < 0.01$, $^{***}p < 0.001$ by one-way ANOVA and Bonferroni's post hoc analysis. OB, olfactory bulb; PFC, prefrontal cortex; STR, striatum; Hippo, dorsal hippocampus; TH, thalamus; HY, hypothalamus; CB, cerebellum, MB, midbrain.

2.4. Immunohistochemistry (IHC) staining

Whole mice brains were fixed in 4% PFA, embedded in wax and sectioned (3μm in thickness). After antigen retrieval with sodium citrate, sections were blocked in 3% hydrogen peroxide for 10 min. Primary antibody working dilutions used were as follows: anti-GFAP (Cat#3670, 1:200, Cell Signaling Technology, USA), Anti-Iba1 antibody (Cat#ab178846, 1:200, Abcam, USA), anti-NeuN (Cat#ab104224, 1:500, Abcam, USA), Anti-8-Hydroxy-2′-deoxyguanosine antibody (Cat#ab48508, 1:500, Abcam, USA). After incubating with primary antibodies, sections were developed with DAB kit (Cat#CW2069, CW bio, China). Images were captured using a microscope (CX23, Olympus, Japan).

2.5. Transmission electron microscope (TEM) analysis

TEM analysis was performed as described in our previous studies (Ding et al., 2020). Briefly, mice brain tissues containing hypothalamus were pre-fixed with 3% glutaraldehyde for 8 h before post-fixing in mixed 1% potassium ferrocyanide and 1% osmium tetroxide for 2 h. Tissues were incubated in Epon resin for 48 h before sectioning (7 nm in thickness). Sections were picked up with copper grids and then observed under a Tecnai G2 electron microscope (FEI, USA) with a CCD camera.

2.6. Spine morphology imaging analysis

Lucifer Yellow dye was used to visualize spine morphology as described before (Ding et al., 2021). Briefly, mice brain tissues were acquired and fixed in 4% PFA for 8 hrs. Brain sections (250μm in thickness) were obtained using a microtome (VT 1200, Leica, Germany). The 4% Lucifer Yellow dye (L0259, Sigma-Aldrich, Germany) was injected into the HY neurons using a micropipette. Morphology of the neurons was visualized with a confocal microscope (FV3000, Nikon, Japan). Three mice per group and 3 neurons per mouse were used in the experiment.

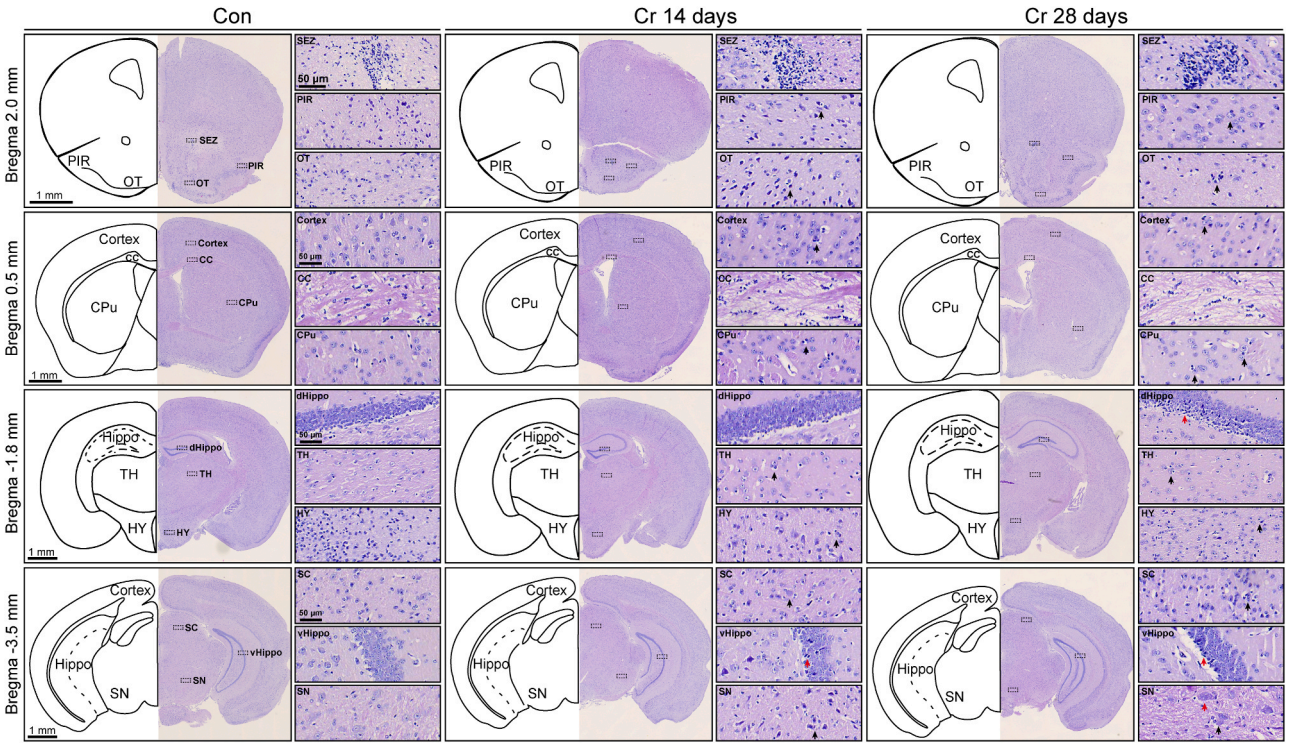

Fig. 2. Representative HE staining in cerebral slices. Different brain areas were shown in coronal section at the level of bregma 2.0 mm, 0.5 mm, −1.8 mm and −3.5 mm. Left, overview of the coronal sections of mice brain; Right, areas enlarged from the left. Black arrows indicated neuronophagia; Red arrows indicated neuronal necrosis. SEZ, subependymal zone; PIR, piriform area; OT, olfactory tubercle; CC, corpus callosum; CPu, caudate putamen; dHippo, dorsal hippocampus; TH, thalamus; HY, hypothalamus; SC, superior colliculus; vhippo, ventral hippocampus; SN, substantia nigra.

2.7. Immunoblots assay

Briefly, brain HY tissue was acquired and homogenized in an extraction buffer. Protein concentration in the supernatant was quantified. A loading buffer was added to the samples before boiling at 99 ^{0}C for 10 min. Proteins were separated by SDS-PAGE before transferring onto PVDF membranes (IPVH 00010, Merck Millipore, Darmstadt, Germany). Targeted protein bands were assessed by using antibodies such as IL-1β (ab9722, 1:500 dilution, Abcam, UK), Nrf2 (ab62352, 1:1000 dilution, Abcam, UK), Nqo-1 (ab80588, 1:2000 dilution, Abcam, UK), Ho-1 (ab189491, 1:1000 dilution, Abcam, UK), 8-OHdG (bs-1278R, 1:500 dilution, Bioss, Beijing, China), NF-κB (ab32536, 1:1000 dilution, Abcam, UK), Lamin B1 (ab16048, 1:1000 dilution, Abcam, UK), IL-6 (ab208113, 1:1000 dilution, Abcam, UK), TNF-α (bs-2081R, 1:1000 dilution, Bioss, China), Claudin5 (35–2500, 1:1000 dilution, Invitrogen, USA), Occludin (ab216327, 1:1000 dilution, Abcam, UK), PSD95 (ab238135, 1:1000 dilution, Abcam, UK), Synaptophysin (ab32127, 1:1000 dilution, Abcam, UK) and β-actin (ab8226, 1:2000 dilution, Abcam, UK). Membranes were incubated overnight with primary antibodies at 4 ℃., then with appropriate secondary antibodies, horseradish peroxidase (HRP) conjugated goat anti-mouse IgG antibody (91196, 1:10000 dilution, CST technology, USA) or HRP conjugated goat anti-rabbit IgG antibody (ab6721, 1:10000 dilution, Abcam, USA). Membranes were developed with electrochemiluminescence reagents to reveal signals. All protein expression levels were normalized to β-actin or Lamin B1.

2.8. Statistical analysis

All data was expressed as mean ± standard error of mean (M ± SEM). All tests were replicated for 3 times. For comparisons among the three groups, one-way ANOVA followed by Berferroni's multiple comparisons test using SPSS version 22.0 (IBM, New York, USA) and GraphPad 8 (GraphPad, USA) were used. Significance was accepted at $p < 0.05$. Statistical parameters, including F and p values, and analytical method used for each analysis are listed in figure legends.

3. Results

3.1. Spatial distribution of chromium in mice cerebrum

Local distribution of Cr was determined by ICP and illustrated in the sketch map (Fig. 1A). We found that the Cr level was increased in multiple brain regions after Cr (VI) exposure (Fig. 1B). The region of highest Cr level in control mice (basal level) was HY, which is 1.9 ppm. The region of highest Cr level in Cr mice was also HY, which is 61.9 ppm (14 days Cr exposure) and 120.9 ppm (28 days Cr exposure). In most brain regions, the Cr level was higher in mice group of 28 days Cr than that of 14 days Cr.

3.2. Cr (VI) induced cerebral pathologies found by HE staining

Next, we tested cerebral pathologies of chromium treated mice. The control mice showed no histological abnormalities in different cerebral areas. The Cr 14 days group mice showed slight neuronophagia and neuronal necrosis in the gray matter of various regions such as hippocampus, cortex, and HY. The white matter such as CC area showed disperse neurites. In the 28-day Cr treated mice, there were large amount of vacuolated neurons, diffuse neuronal necrosis, neuronal pyknosis and neuronophagia in gray matter especially in HY, hippocampus and cortex. Moreover, the CC area showed vacuolization in neurites (Fig. 2).

3.3. Cr (VI) raised astrocyte activation in areas of cerebrum

We performed GFAP IHC staining to test the astrocyte number in

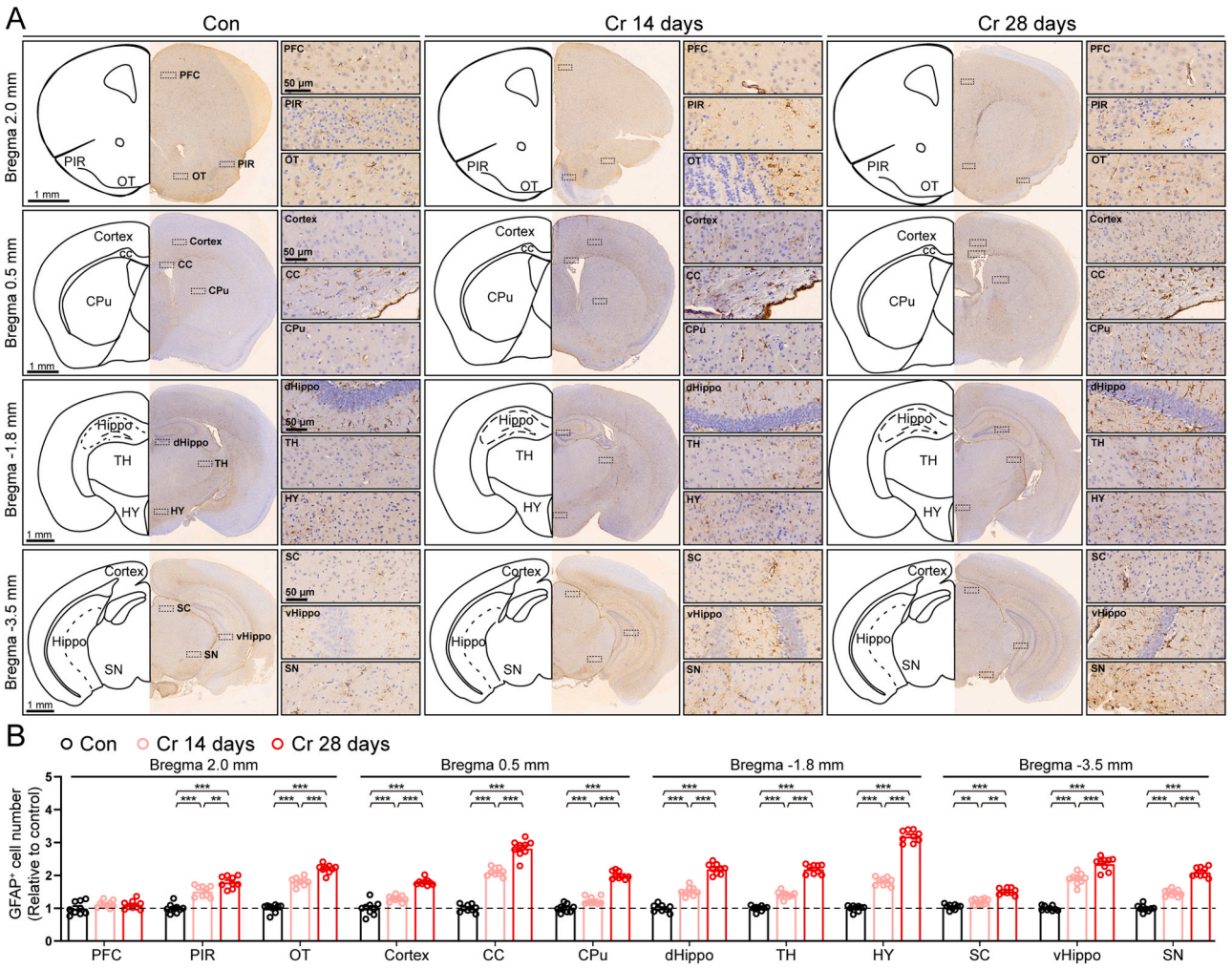

Fig. 3. Effect of chromium on astrocyte activation. (A) Representative GFAP IHC staining of different brain areas in coronal section at the level of bregma 2.0 mm, 0.5 mm, −1.8 mm and −3.5 mm. (B) Stereological counts of GFAP$^+$ cells. PFC: F (2, 26) = 1.699, P = 0.204, PIR: F (2, 26) = 56.079, P < 0.001, OT: F (2, 26) = 205.314, P < 0.001, Cortex: F (2, 26) = 69.574, P < 0.001, CC: F (2, 26) = 242.822, P < 0.001, CPu: F (2, 26) = 177.898, P < 0.001, dHippo: F (2, 26) = 173.567, P < 0.001, TH: F (2, 26) = 262.789, P < 0.001, HY: F (2, 26) = 614.895, P < 0.001, SC: F (2, 26) = 67.46, P < 0.001, vHippo: F (2, 26) = 173.758, P < 0.001, SN: F (2, 26) = 196.01, P < 0.001. n = 9 mice, *p < 0.05, **p < 0.01, ***p < 0.001 by one-way ANOVA and Bonferroni's post hoc analysis. PFC, prefrontal cortex; PIR, piriform area; OT, olfactory tubercle; CC, corpus callosum; CPu, caudate putamen; dHippo, dorsal hippocampus; TH, thalamus; HY, hypothalamus; SC, superior colliculus; vhippo, ventral hippocampus; SN, substantia nigra.

mice brains treated with Cr (VI). The number of GFAP positive cells was increased in cerebral areas such as PIR, OT, Cortex, CC, CPu, dHippo, TH, HY, SC, vHippo and SN after Cr exposure. Notably, we observed a 3.19-fold increase of GFAP positive cells in HY area of 28-days Cr treated mice, which was the highest increasing rate among those cerebral areas (Fig. 3A, B), when compared with the control mice. Moreover, we found that the astrocyte processes were highly branched in chromium treated mice.

3.4. Cr (VI) induced microglial activation in cerebrum

To determine the extent of Cr induced microglial activation, we examined GFAP positive astrocytes by immunostaining. We found that the microglia number increased in multiple brain regions including PFC, PIR, OT, Cortex, CC, CPu, dHippo, TH, HY, SC, vHippo and SN areas after 28 days Cr exposure (Fig. 4A, B). Note that the area of highest increase in astrocytic number was HY (about 3.11 fold to control). And the cell bodies of microglia were hypertrophied in both 14-day and 28-day chromium exposed mice than that in control mice.

3.5. Cr (VI) induced neuronal loss in HY

Since the astrocyte and microglial activation were more remarkable in HY than that in other cerebral regions, we next tested the degree of neurodegeneration in HY with IHC staining using NeuN (a specific neuronal marker). We found that the neuronal number in HY, but not other regions, was decreased than that in chromium treatment group mice (Fig. 5A, B).

3.6. Cr (VI) induced BBB breakdown in HY

To assess the effects of chromium exposure on BBB integrity, we conducted TEM to observe the ultrastructure of BBB. We found chromium treatment induced a lower TJ number, a higher astrocyte end-feet area and a lower pericyte coverage compared with the control mice (Fig. 6A, B, C, D). Note that, the astrocyte end-feet area was higher in 28-day Cr group than that in 14-day group. The pericyte coverage and tight junctions were found lower in number when treated for 28 days than that in 14 days. We next evaluated the tight junction protein (Claudin5 and Occludin) levels after chromium exposure. Both exposure duration of 14 days and 28 days significantly reduced the endothelial tight

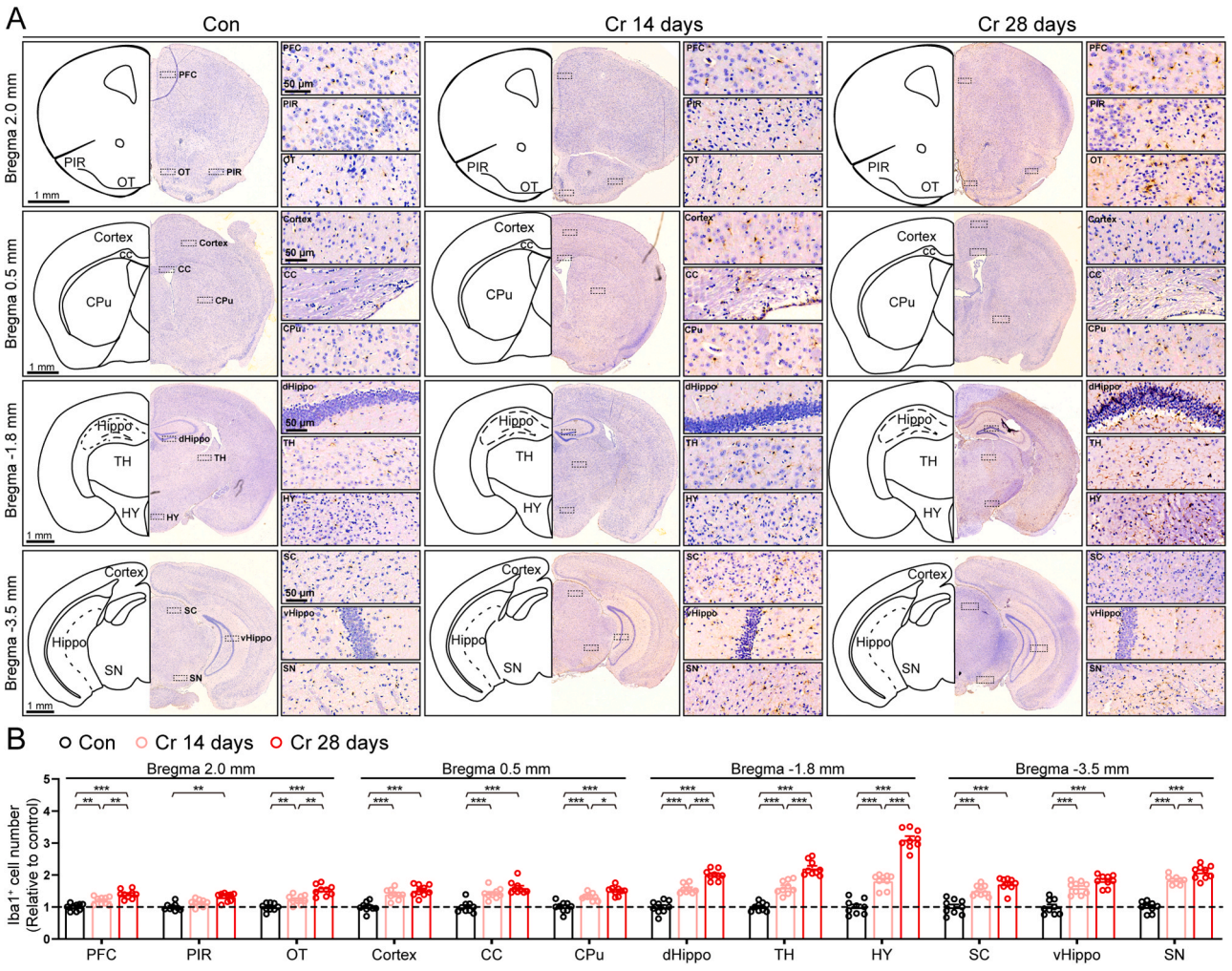

Fig. 4. Effect of chromium on microglia activation. (A) Representative Iba1 IHC staining of different brain areas in coronal section at the level of bregma 2.0 mm, 0.5 mm, −1.8 mm and −3.5 mm. (B) Stereological counts of Iba1^{+} cells. PFC: F (2, 26) = 23.704, $P < 0.001$, PIR: F (2, 26) = 15.464, $P < 0.001$, OT: F (2, 26) = 28.997, $P < 0.001$, Cortex: F (2, 26) = 24.002, $P < 0.001$, CC: F (2, 26) = 25.823, $P < 0.001$, CPu: F (2, 26) = 30.161, $P < 0.001$, dHippo: F (2, 26) = 79.964, $P < 0.001$, TH: F (2, 26) = 85.271, $P < 0.001$, HY: F (2, 26) = 163.223, $P < 0.001$, SC: F (2, 26) = 30.226, $P < 0.001$, vHippo: F (2, 26) = 38.647, $P < 0.001$, SN: F (2, 26) = 99.504, $P < 0.001$. n = 9 mice, $^{*}p < 0.05$, $^{**}p < 0.01$, $^{***}p < 0.001$ by one-way ANOVA and Bonferroni's post hoc analysis. PFC, prefrontal cortex; PIR, piriform area; OT, olfactory tubercle; CC, corpus callosum; CPu, caudate putamen; dHippo, dorsal hippocampus; TH, thalamus; HY, hypothalamus; SC, superior colliculus; vHippo, ventral hippocampus; SN, substantia nigra.

junction protein levels compared with the control mice (Fig. 6E, F, G). Note that the tight junction protein levels were much lower in 28 days treatment group than that in 14 days group.

3.7. Cr (VI) induced axonal and spine degeneration, neuronal oxidative stress, and inflammatory factors accumulation in HY

We next examined the effect of Cr on axonal and dendritic morphologies in HY. Using silver stain to analyze the intensity of axons, we found the axonal intensity was lower after Cr exposure. Notably, the axonal pathology was more severe in 28-day Cr group than that in 14 days (Fig. 7A, C). Next, we tested the spinal morphology using lucifer yellow intracellular injection. We found loss of total spine, mushroom-type spine and thin-type spine in both 14-day and 28-day Cr groups compared with that in control group (Fig. 7B, D, E, F). Moreover, TEM results showed a loss of synaptic number, a shorter PSD length and a lower PSD thickness in both14-day and 28-day Cr groups compared with that in control group. Note that the synaptic number, PSD length and PSD thickness was lower in 28-day Cr group than that in 14-day Cr group (Fig. 7G, H, I, J). Immunoblotting assay showed synaptic proteins (PSD95 and Syn) levels were decreased after Cr exposure (Fig. 7K, L).

To determine the extent of Cr induced oxidative stress in mice brains, the 8-OHdG IHC staining was conducted. We found higher 8-OHdG intensity in HY, Cortex, and dHippo areas in Cr exposed brains with the highest in HY (Fig. 8A, B). Next, we conducted immunobloting of the Nrf2 related oxidative stress markers. We found nuclear Nrf2 was reduced, and Nqo-1, Ho-1 and 8-OHdG were increased after Cr (VI) exposure (Fig. 8C, D, E, F).

Then we analyzed the levels of NF-κB related inflammatory pathway makers, including IL-1β, IL-6 and TNF-α. We found that the nuclear NF-κB, IL-1β, IL-6 and TNF-α levels were markedly increased after Cr (VI) intoxication. Note the levels of NF-κB, IL-1β, IL-6 and TNF-α in the 28-day Cr exposure group were much higher than that in the 14-day Cr exposure group (Fig. 8G, H, I, J).

4. Discussion

In the present study, we first evaluated whether hexavalent Cr (VI) could enter the brain through intraperitoneally administration. We found that Cr (VI) may enter the brain through BBB in the HY. Meanwhile, the Cr (VI) could destruct the BBB integrity by damaging the pericytes and reducing tight junction proteins. Moreover, we found that

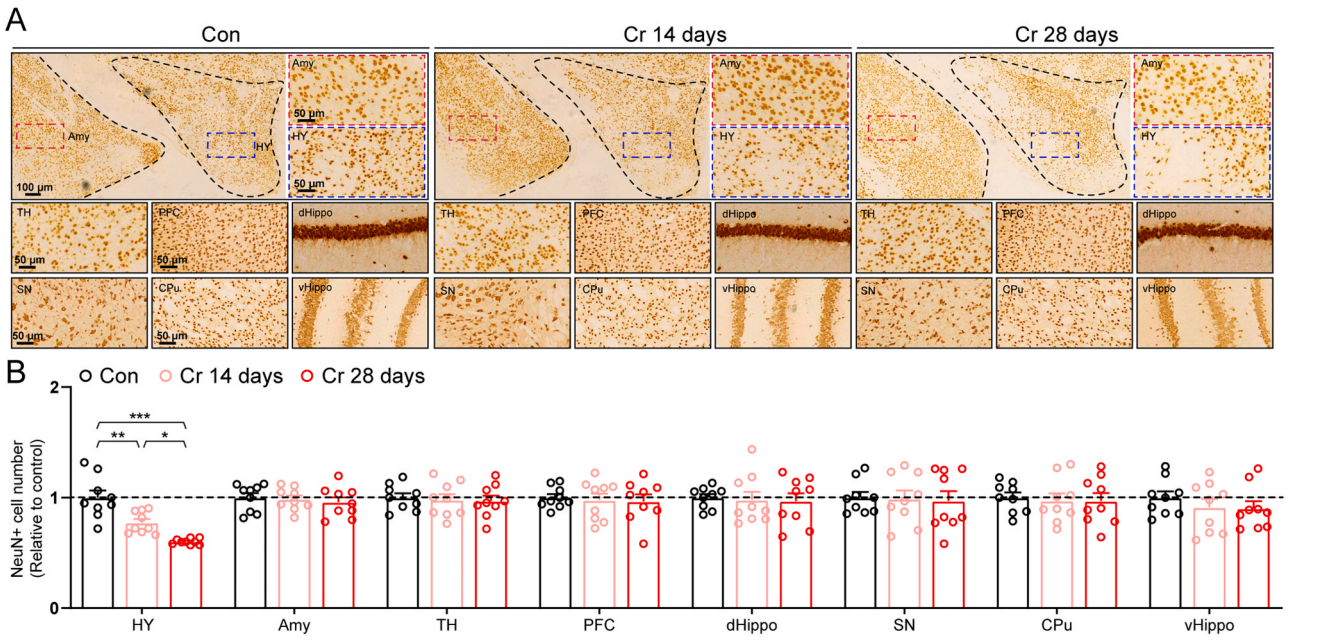

Fig. 5. Effect of chromium on neuronal number in different brain regions. (A) Representative NeuN IHC staining of different brain areas in coronal section at the level of bregma 2.0 mm, 0.5 mm, −1.8 mm and −3.5 mm. (B) Stereological counts of NeuN$^+$ cells. HY: F (2, 26) = 22.989, $P < 0.001$, Amy: F (2, 26) = 0.271, P = 0.765, TH: F (2, 26) = 0.118, P = 0.889, PFC: F (2, 26) = 0.102, P = 0.903, dHippo: F (2, 26) = 0.07, P = 0.933, SN: F (2, 26) = 0.045, P = 0.956, CPu: F (2, 26) = 0.077, P = 0.926, vHippo: F (2, 26) = 0.668, P = 0.522. n = 9 mice, *$p < 0.05$, **$p < 0.01$, ***$p < 0.001$ by one-way ANOVA and Bonferroni's post hoc analysis. HY, hypothalamus; Amy, amygdala, TH, thalamus; PFC, prefrontal cortex; dHippo, dorsal hippocampus; SN, substantia nigra; CPu, caudate putamen; vHippo, ventral hippocampus.

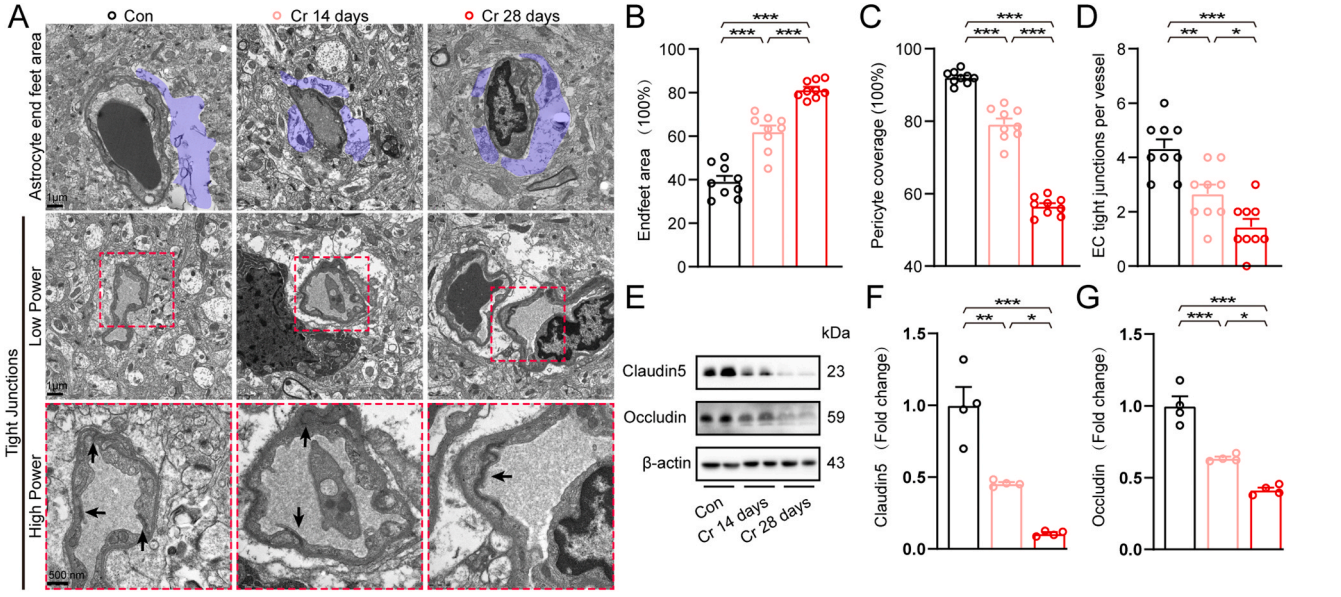

Fig. 6. Cr triggered BBB breakdown and TJ loss. (A) TEM images of astrocyte endfeet and TJ morphologies of BBB in HY. (B) Analysis of astrocyte end feet area. n = 9 mice, F (2, 26) = 85.958, $P < 0.001$. (C) Analysis of pericyte coverage. n = 9 mice, F (2, 26) = 293.442, $P < 0.001$. (D) Analysis of TJ per vessel. n = 9 mice, F (2, 26) = 20.44, $P < 0.001$. (E) Immunoblots of Claudin5 and Occludin in HY. (F) Quantification of Claudin5. n = 4 mice, F (2, 11) = 37.159, $P < 0.001$. (G) Quantification of Occuludin. n = 4 mice, F (2, 11) = 54.604, $P < 0.001$. *$p < 0.05$, **$p < 0.01$, ***$p < 0.001$ by one-way ANOVA and Bonferroni's post hoc analysis.

Cr (VI) was specifically accumulated in HY over time when two different exposure durations (14 days and 28 days) of Cr (VI) were applied in mice. And the accumulated Cr could induce gliosis in multiple brain regions especially in HY area. These were consistent with recent studies (Hegazy et al., 2021; Wise et al., 2022). The Cr (VI) exposure could lead to axonal and dendritic degeneration and neuronal number loss in HY. Finally, the Nrf2 related antioxidant system and NF-κB related inflammatory signaling might mediate the neuropathology induced by Cr (VI) exposure.

Many Cr (VI) exposure routes, including intraperitoneal, oral, and intratracheal, were used for studying Cr (VI) neurotoxicity in different species (Heffern et al., 2018; Hegazy et al., 2021; Mahmoud and Abd El-Twab, 2017; Mate et al., 2017; Ueno et al., 2001). However, whether Cr (VI) could cross BBB, or damage it, remained inconsistent across studies. Thus, intranasal Cr (VI) administration was generally used to verify whether the intracerebral Cr (VI) accumulation was through the

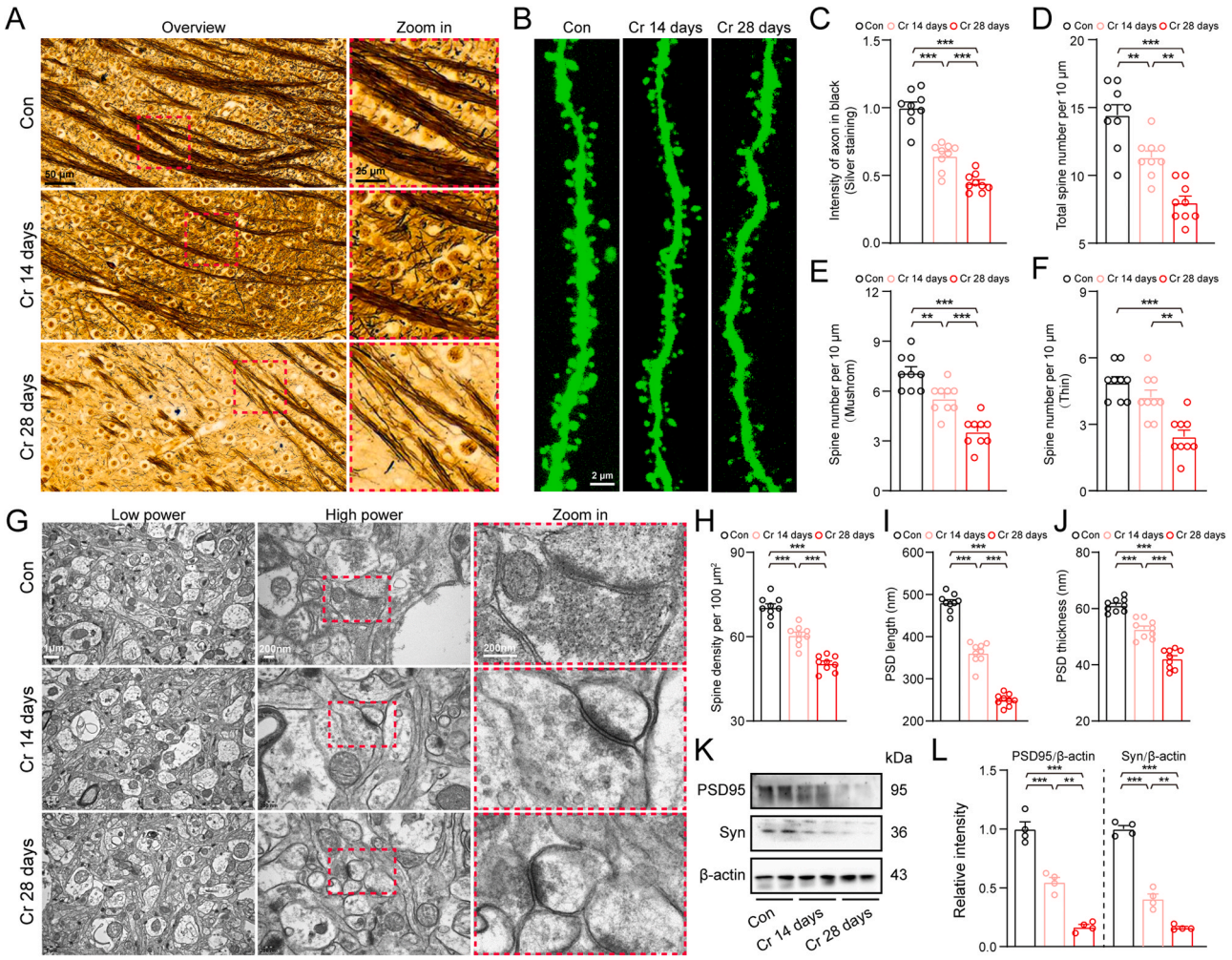

Fig. 7. Cr induced axonal and synaptic degeneration in HY. (A) Representative images of silver staining in HY. (B) Representative images of spines by Lucifer Yellow intra-neuronal injection in HY neurons. (C) Intensity of axons analysis. n=9 mice, F (2, 26) = 71.317, $P < 0.001$. (D) Quantification of total spine number in HY. (E) Quantification of mushroom-type spine number. n=9 mice, F (2, 26) = 30.228, $P < 0.001$. (F) Quantification of thin-type spine number. n=9 mice, F (2, 26) = 32.167, $P < 0.001$. (G) Representative TEM micrographs of synapses in HY. n=9 mice, F (2, 26) = 18.476, $P < 0.001$. (H) Quantification of synaptic density in HY. n=9 mice, F (2, 26) = 79.803, $P < 0.001$. (I) Quantification of PSD length in HY. n=9 mice, F (2, 26) = 282.886, $P < 0.001$. (J) Quantification of PSD thickness in HY. n=9 mice, F (2, 26) = 85.936, $P < 0.001$. (K) Immunoblots of TJ proteins PSD95 and Syn of HY. (L) Analysis of PSD95 and Syn levels. n=4 mice, PSD95: F (2, 11) = 89.113, $P < 0.001$, Syn: F (2, 11) = 207.462, $P < 0.001$. $^{*}p < 0.05$, $^{**}p < 0.01$, $^{***}p < 0.001$ by one-way ANOVA and Bonferroni's post hoc analysis.

olfactory bulb, which is unprotected by the BBB (Salama and Elgohary, 2021; Sedik and Elgohary, 2023; Wang et al., 2022). In this work we detected the spatial Cr (VI) distribution in cerebral regions including OB, PFC, STR, Hippo, TH, HY, CB, MB and medulla. The exogenous Cr (VI) was mainly accumulated in HY area among those brain regions. Moreover, we found that the hypothalamic Cr (VI) level was increased over time when Cr (VI) exposures were scheduled differently. The HY, which constitutes the HPA axis, functions as an endocrine organ by releasing endocrine hormones into the blood. The BBB is much weaker in HY among other brain regions so that secretory cells are easier to interact with blood (Abdel-Rahman et al., 2023). Thus, we concluded that the HY was the gate for Cr (VI) to enter the brain.

The effects of Cr (VI) on BBB were not reported before. Thus we analyzed the BBB morphology and tight junction (TJ) proteins using TEM and immunoblot. We found that the BBB integrity was compromised, and tight junction proteins were lost in Cr (VI) exposed mice HY areas. Previous studies showed Cr (VI) could affect human umbilical vein endothelial cells to recruit peripheral inflammatory cells (Cao et al., 2020). We reckoned that Cr (VI) could disrupt the tight junction proteins of brain vascular endothelial cells, leading to hypothalamic BBB breakdown. The Cr (VI) induced BBB dysfunction made it easier for Cr (VI) to cross the BBB. These two processes formed a vicious cycle.

The HE staining results revealed a timely dependent Cr (VI) induced neuropathology in mice. Morphologically, neuronophagia and neuronal necrosis were observed in Cr (VI) treated mice brains. The longer Cr (VI) exposure (28 days versus 14 days) the more severe neuropathologies were observed. Correspondingly, recent studies showed that either longer Cr (VI) exposure or higher dose administration created more destruction (Hegazy et al., 2021). These results were also observed in Cr (VI) exposed human (Block and Calderon-Garciduenas, 2009).

Similarly, a time dependent Cr (VI) induced gliosis was observed in Cr (VI) mice especially in HY areas. The hypothalamic Cr (VI), which came across from blood, could recruit inflammatory cells. Thus, the number of local glial cells increased along with time when exposed with two time schedule. The activated glial cells, which secret inflammatory factors including IL-1β and TNF-α, might increase neuronal mortality rate (Ding et al., 2022). Thus, we observed hypothalamic neuronal number loss, axonal degeneration and synaptic loss as shown by NeuN IHC, silver staining and TEM analysis respectively. Note that the neuronal numbers in other brain regions were not comparable. We thought that the gliosis was triggered by local Cr. The higher concentration of local Cr, the more severe gliosis was observed.

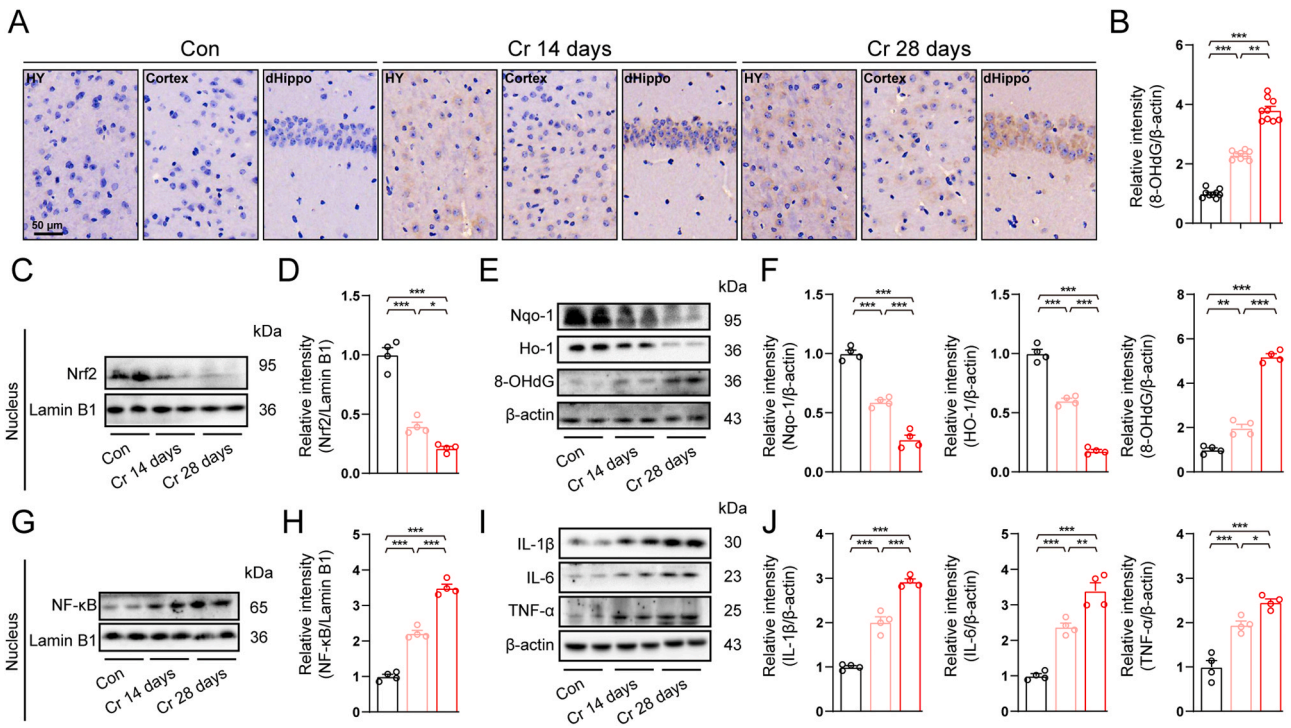

Fig. 8. Effect of chromium on Nrf2 related oxidative stress signaling and NF-κB related inflammatory pathway. (A) Representative images of 8-OHdG IHC staining in HY, cortex and Hippo. (B) Relative intensity of 8-OHdG from IHC staining results. n=9 mice, F (2, 26) = 282.07, $P < 0.001$. (C) Immunoblots of nuclear Nrf2. (D) Analysis of nuclear Nrf2 relative levels. n=4 mice, F (2, 11) = 101.151, $P < 0.001$. (E) Immunoblots of Nqo-1, Ho-1, 8-OHdG in HY. (F) Analysis of Nqo-1, Ho-1, 8-OHdG relative levels in HY. n=4 mice, Nqo-1: F (2, 11) = 154.397, $P < 0.001$, Ho-1: F (2, 11) = 281.024, $P < 0.001$, 8-OHdG: F (2, 11) = 275.44, $P < 0.001$. (G) Immunoblots of nuclear NF-κB. (H) Analysis of nuclear NF-κB relative levels. n=4 mice, F (2, 11) = 223.898, $P < 0.001$. (I) Immunoblots of IL-1β, IL-6 and TNF-α in HY. (J) Analysis of IL-1β, IL-6 and TNF-α relative levels in HY. n=4 mice, IL-1β: F (2, 11) = 153.391, $P < 0.001$, IL-6: F (2, 11) = 64.082, $P < 0.001$, TNF-α: F (2, 11) = 46.77, $P < 0.001$. $^{*}p < 0.05$, $^{**}p < 0.01$, $^{***}p < 0.001$ by one-way ANOVA and Bonferroni's post hoc analysis.

To further determine the mechanism of Cr (VI) induced neuropathology in HY, we conducted IHC staining of 8-OHdG which is a DNA damage marker induced by ROS. Previous studies showed that Cr (VI) typically induces oxidative damage and ROS in brain (Zhang et al., 2023b). The ROS and oxidative stress produces redox homeostasis, leading to DNA and cellular lipids damaged (Saleh et al., 2022). A significant difference of 8-OHdG intensity were observed in control, 14-day Cr(VI), and 28-day Cr (VI) groups. A recent study showed that intratracheal exposure of hexavalent chromium may induce DNA damage in the lungs through activation of the PI3K-Akt signaling pathway (Zhang et al., 2023a).

Based on the above data, we next evaluated the neuropathologies in HY in Cr (VI) exposed mice. We focused on the processes of axons and dendrites. Compromised axons, dendritic spines and synapses were observed in HY of Cr (VI) exposed mice. Thus we reckoned that the local Cr might potentiate the neuropaghology in HY.

The Nrf2 pathway was involved in numerous heavy metal intoxications, such as iron (Piloni et al., 2021), Zinc (Arisumi et al., 2023), arsenic (Najafi et al., 2023), manganese (Ijomone et al., 2022), etc. We hypothesized that Cr might induce the reduction of nuclear localization of Nrf2, leading to the antioxidant system dysfunction. To validate our hypothesis, we tested nuclear Nrf2 and cytoplasmic antioxidant enzymes in HY. As expected, we found the nuclear Nrf2 and cytoplasmic antioxidant enzymes were markedly reduced after Cr (VI) intoxication. Thus, it is highly conceivable that the Nrf2 pathway was suppressed after Cr (VI) exposure. Therefore, targeting Nrf2 might alleviate chromium-induced brain injury (Sedik and Elgohary, 2023).

Neuroinflammation was common in heavy metal intoxication (Murumulla et al., 2023). We found that the inflammatory factors, which were regulated by NF-κB transcription factor, were increased in Cr (VI) mice model. Our data strongly support and essential role for NF-κB signaling in transcription of neuronal inflammatory factors.

It is important to note the limitation of our study. First, we did not investigate the vulnerable cell types affected by Cr (VI) in HY. Second, we did not carry out any behavioral analysis of Cr (VI) treated mice. Third, although we have shown that the HY is the Cr (VI)-vulnerable brain region, we did not test the hypothalamic hormone levels. Future investigation of these issues is warranted and may provide the exact mechanism of Cr-induced neuropathology in HY.

In conclusion, our data suggests that 1) the HY is the Cr (VI)-vulnerable brain region; 2) The concentration of Cr was the highest in HY after Cr (VI) exposure; 3) Cr (VI) might enter the brain parenchyma across BBB; 4) The BBB of HY was disrupted after Cr accumulation; 5) The local Cr in HY induced neuropathology might be through the Nrf2 related antioxidant system and NF-κB related inflammatory signaling. These findings may offer therapeutic opportunities for Cr (VI) induced neuropathology.

Ethics statement

The animal study was reviewed and approved by Guizhou Medical University.

Funding

This work was supported by Department of Education of Guizhou Province (Guizhou Teaching and Technology [2023] 015) to BFS, Guizhou Provincial Science and Technology Program Project (Grant No. Qiankehe Platform Talents-GCC [2023] 035), Guizhou Science and Technology Plan Project (Grant No. Guizhou Science Support [2023] General 232), National Natural Science Foundation of China (Grant No. 82260263) (to XLQ).

CRediT authorship contribution statement

Jiuyang Ding: Writing – original draft, Methodology, Investigation. **Yunle Meng:** Project administration. **Bing Xia:** Project administration. **shanshan Hu:** Project administration. **Xueyu Jiang:** Project administration. **Changyou Liu:** Validation, Project administration. **Juan Zheng:** Validation, Project administration. **Jiawen Wang:** Resources, Conceptualization. **Yingdong Gao:** Validation, Project administration. **Xiaolan Qi:** Writing – review & editing, Funding acquisition, Conceptualization. **Baofei Sun:** Writing – review & editing, Writing – original draft, Methodology, Investigation, Funding acquisition. **Zhihui Dai:** Resources, Conceptualization. **Xianglin Pei:** Project administration. **Nannan Jia:** Project administration. **Jian Huang:** Project administration.

Declaration of Competing Interest

The authors declare that they have no known competing financial interests or personal relationships that could have appeared to influence the work reported in this paper.

Data availability

Data will be made available on request.

References

Abdel-Rahman, M., Elmasry, H.M., Ahmed-Farid, O.A., Hegazy, S.M., Rezk, M.M., 2023. Neurological study on the effect of CeNPs and/or La Cl(3) on adult male albino rats. J. Trace Elem. Med. Biol. 81, 127323 https://doi.org/10.1016/j.jtemb.2023.127323.

Arisumi, S., Fujiwara, T., Yasumoto, K., Tsutsui, T., Saiwai, H., Kobayakawa, K., Okada, S., Zhao, H., Nakashima, Y., 2023. Metallothionein 3 promotes osteoclast differentiation and survival by regulating the intracellular Zn(2+) concentration and NRF2 pathway. Cell Death Discov. 9, 436. https://doi.org/10.1038/s41420-023-01729-y.

Block, M.L., Calderon-Garciduenas, L., 2009. Air pollution: mechanisms of neuroinflammation and CNS disease. Trends Neurosci. 32, 506–516. https://doi.org/10.1016/j.tins.2009.05.009.

Calderon-Garciduenas, L., Serrano-Sierra, A., Torres-Jardon, R., Zhu, H., Yuan, Y., Smith, D., Delgado-Chavez, R., Cross, J.V., Medina-Cortina, H., Kavanaugh, M., Guilarte, T.R., 2013. The impact of environmental metals in young urbanites' brains. Exp. Toxicol. Pathol. 65, 503–511. https://doi.org/10.1016/j.etp.2012.02.006.

Cao, X., Bi, R., Hao, J., Wang, S., Huo, Y., Demoz, R.M., Banda, R., Tian, S., Xin, C., Fu, M., Pi, J., Liu, J., 2020. A study on the protective effects of taxifolin on human umbilical vein endothelial cells and THP-1 cells damaged by hexavalent chromium: a probable mechanism for preventing cardiovascular disease induced by heavy metals. Food Funct. 11, 3851–3859. https://doi.org/10.1039/d0fo00567c.

Carrera-Gonzalez, M.D.P., Canton-Habas, V., Rich-Ruiz, M., 2022. Aging, depression and dementia: the inflammatory process. Adv. Clin. Exp. Med. 31, 469–473. https://doi.org/10.17219/acem/149897.

Civit, T., Houdayer, A.J., Kennedy, G., 2000. A search for trace elements in some human intracranial tumors by instrumental neutron activation analysis. Biol. Trace Elem. Res. 74, 203–210. https://doi.org/10.1385/BTER:74:3:203.

DesMarais, T.L., Costa, M., 2019. Mechanisms of chromium-induced toxicity. Curr. Opin. Toxicol. 14, 1–7. https://doi.org/10.1016/j.cotox.2019.05.003.

Ding, J., Lian, Y., Meng, Y., He, Y., Fan, H., Li, C., Qiu, P., 2020. The effect of alpha-synuclein and Tau in methamphetamine induced neurotoxicity in vivo and in vitro. Toxicol. Lett. 319, 213–224. https://doi.org/10.1016/j.toxlet.2019.11.028.

Ding, J., Huang, J., Xia, B., Hu, S., Fan, H., Dai, J., Li, Z., Wang, J., Le, C., Qiu, P., Wang, Y., 2021. Transfer of alpha-synuclein from neurons to oligodendrocytes triggers myelin sheath destruction in methamphetamine administration mice. Toxicol. Lett. 352, 34–45. https://doi.org/10.1016/j.toxlet.2021.09.005.

Ding, J., Shen, L., Ye, Y., Hu, S., Ren, Z., Liu, T., Dai, J., Li, Z., Wang, J., Luo, Y., Zhang, Q., Zhang, X., Qi, X., Huang, J., 2022. Inflammasome inhibition prevents motor deficit and cerebellar degeneration induced by chronic methamphetamine administration. Front. Mol. Neurosci. 15, 861340 https://doi.org/10.3389/fnmol.2022.861340.

Doker, S., Mounicou, S., Dogan, M., Lobinski, R., 2010. Probing the metal-homeostatis effects of the administration of chromium(vi) to mice by ICP MS and size-exclusion chromatography-ICP MS. Metallomics 2, 549–555. https://doi.org/10.1039/c004508j.

Grochowski, C., Blicharska, E., Krukow, P., Jonak, K., Maciejewski, M., Szczepanek, D., Jonak, K., Flieger, J., Maciejewski, R., 2019. Analysis of trace elements in human brain: its aim, methods, and concentration levels. Front. Chem. 7, 115. https://doi.org/10.3389/fchem.2019.00115.

Haddad-Tovolli, R., Dragano, N.R.V., Ramalho, A.F.S., Velloso, L.A., 2017. Development and function of the blood-brain barrier in the context of metabolic control. Front. Neurosci. 11, 224. https://doi.org/10.3389/fnins.2017.00224.

Hanson, L.R., Frey 2nd, W.H., 2008. Intranasal delivery bypasses the blood-brain barrier to target therapeutic agents to the central nervous system and treat neurodegenerative disease. BMC Neurosci. 9 (Suppl 3), S5 https://doi.org/10.1186/1471-2202-9-s3-s5.

Heffern, K., Tierney, K., Gallagher, E.P., 2018. Comparative effects of cadmium, zinc, arsenic and chromium on olfactory-mediated neurobehavior and gene expression in larval zebrafish (*Danio rerio*). Aquat. Toxicol. 201, 83–90. https://doi.org/10.1016/j.aquatox.2018.05.016.

Hegazy, R., Mansour, D., Salama, A., Hassan, A., Saleh, D., 2021. Exposure to intranasal chromium triggers dose and time-dependent behavioral and neurotoxicological defects in rats. Ecotoxicol. Environ. Saf. 216, 112220 https://doi.org/10.1016/j.ecoenv.2021.112220.

Holmes, A.L., Wise, S.S., Wise Sr., J.P., 2008. Carcinogenicity of hexavalent chromium. Indian J. Med. Res. 128, 353–372.

Huang, T., Liu, L.F., Zhou, L.L., Zhang, S.W., 2018. Electrokinetic removal of chromium from chromite ore-processing residue using graphite particle-supported nanoscale zero-valent iron as the three-dimensional electrode. Chem. Eng. J. 350, 1022–1034. https://doi.org/10.1016/j.cej.2018.06.048.

Huang, T., Song, D., Yin, L.X., Zhang, S.W., Liu, L.F., Zhou, L., 2020. Microwave irradiation assisted sodium hexametaphosphate modification on the alkali-activated blast furnace slag for enhancing immobilization of strontium. Chemosphere 241, 125069. https://doi.org/10.1016/j.chemosphere.2019.125069.

Huang, T., Zhang, S.W., Liu, L.F., Zhou, L., 2021. Green rust functionalized geopolymer of composite cementitious materials and its application on treating chromate in a holistic system. Chemosphere 263, 128319. https://doi.org/10.1016/j.chemosphere.2020.128319.

Huang, T., Pan, L., Dong, J., Zhou, L., Tao, H., Zhang, S.W., Li, A., 2022. A comprehensive investigation of zeolite-rich tuff functionalized with 3-mercapto-propionic acid intercalated green rust for the efficient removal of Hg(II) and Cr(VI) in a binary system. J. Environ. Manag. 324, 116344 https://doi.org/10.1016/j.jenvman.2022.116344.

Ijomone, O.M., Iroegbu, J.D., Morcillo, P., Ayodele, A.J., Ijomone, O.K., Bornhorst, J., Schwerdtle, T., Aschner, M., 2022. Sex-dependent metal accumulation and immunoexpression of Hsp70 and Nrf2 in rats' brain following manganese exposure. Environ. Toxicol. 37, 2167–2177. https://doi.org/10.1002/tox.23583.

Khamirchi, R., Moslem, A., Agah, J., Pozo, O.J., Miri, M., Dadvand, P., 2020. Maternal exposure to air pollution during pregnancy and cortisol level in cord blood. Sci. Total Environ. 713, 136622 https://doi.org/10.1016/j.scitotenv.2020.136622.

Kim, J.H., Byun, H.M., Chung, E.C., Chung, H.Y., Bae, O.N., 2013. Loss of integrity: impairment of the blood-brain barrier in heavy metal-associated ischemic stroke. Toxicol. Res 29, 157–164. https://doi.org/10.5487/tr.2013.29.3.157.

Mahmoud, A.M., Abd El-Twab, S.M., 2017. Caffeic acid phenethyl ester protects the brain against hexavalent chromium toxicity by enhancing endogenous antioxidants and modulating the JAK/STAT signaling pathway. Biomed. Pharm. 91, 303–311. https://doi.org/10.1016/j.biopha.2017.04.073.

Mate, Z., Horvath, E., Papp, A., Kovacs, K., Tombacz, E., Nesztor, D., Szabo, T., Szabo, A., Paulik, E., 2017. Neurotoxic effects of subchronic intratracheal Mn nanoparticle exposure alone and in combination with other welding fume metals in rats. Inhal. Toxicol. 29, 227–238. https://doi.org/10.1080/08958378.2017.1350218.

Murumulla, L., Bandaru, L.J.M., Challa, S., 2023. Heavy metal mediated progressive degeneration and its noxious effects on brain microenvironment. Biol. Trace Elem. Res. https://doi.org/10.1007/s12011-023-03778-x.

Najafi, N., Rezaee, R., Hayes, A.W., Karimi, G., 2023. A review of mechanisms underlying the protective effects of natural compounds against arsenic-induced neurotoxicity. Biometals 36, 799–813. https://doi.org/10.1007/s10534-022-00482-6.

Piloni, N.E., Vargas, R., Fernandez, V., Videla, L.A., Puntarulo, S., 2021. Effects of acute iron overload on Nrf2-related glutathione metabolism in rat brain. Biometals 34, 1017–1027. https://doi.org/10.1007/s10534-021-00324-x.

Qie, Y., Zhou, D., Wu, Z., Liu, S., Shen, C., Hu, H., Zhang, C., Xu, Y., 2022. Low-dose hexavalent chromium(VI) exposure promotes prostate cancer cell proliferation by activating MAGEB2-AR signal pathway. Ecotoxicol. Environ. Saf. 241, 113724 https://doi.org/10.1016/j.ecoenv.2022.113724.

Rajan, M.T., Jagannatha Rao, K.S., Mamatha, B.M., Rao, R.V., Shanmugavelu, P., Menon, R.B., Pavithran, M.V., 1997. Quantification of trace elements in normal human brain by inductively coupled plasma atomic emission spectrometry. J. Neurol. Sci. 146, 153–166. https://doi.org/10.1016/S0022-510X(96)00300-0.

Reale, E., Sandstrom, J., Culot, M., Hechon, J., Wellens, S., Heymans, M., Tschudi-Monnet, F., Vernez, D., Hopf, N.B., 2023. Predicting human neurotoxicity of propylene glycol methyl ether (PGME) by implementing in vitro neurotoxicity results into toxicokinetic modelling. Sci. Total Environ. 886, 163767 https://doi.org/10.1016/j.scitotenv.2023.163767.

Salama, A., Elgohary, R., 2021. L-carnitine and Co Q10 ameliorate potassium dichromate -induced acute brain injury in rats targeting AMPK/AKT/NF-kappabeta. Int. Immunopharmacol. 101, 107867 https://doi.org/10.1016/j.intimp.2021.107867.

Saleh, E.M., Hamdy, G.M., Hassan, R.E., 2022. Neuroprotective effect of sodium alginate against chromium-induced brain damage in rats. PLoS One 17, e0266898. https://doi.org/10.1371/journal.pone.0266898.

Sedik, A.A., Elgohary, R., 2023. Neuroprotective effect of tangeretin against chromium-induced acute brain injury in rats: targeting Nrf2 signaling pathway, inflammatory mediators, and apoptosis. Inflammopharmacology 31, 1465–1480. https://doi.org/10.1007/s10787-023-01167-3.

Shaw, P., Mondal, P., Bandyopadhyay, A., Chattopadhyay, A., 2020. Environmentally relevant concentration of chromium induces nuclear deformities in erythrocytes and

alters the expression of stress-responsive and apoptotic genes in brain of adult zebrafish. Sci. Total Environ. 703, 135622 https://doi.org/10.1016/j.scitotenv.2019.135622.

Ueno, S., Kashimoto, T., Susa, N., Furukawa, Y., Ishii, M., Yokoi, K., Yasuno, M., Sasaki, Y.F., Ueda, J., Nishimura, Y., Sugiyama, M., 2001. Detection of dichromate (VI)-induced DNA strand breaks and formation of paramagnetic chromium in multiple mouse organs. Toxicol. Appl. Pharm. 170, 56–62. https://doi.org/10.1006/taap.2000.9081.

Wang, L., Bayanbold, K., Zhao, L., Wang, Y., Adamcakova-Dodd, A., Thorne, P.S., Yang, H., Jiang, B.H., Liu, L.Z., 2022. Redox sensitive miR-27a/b/Nrf2 signaling in Cr(VI)-induced carcinogenesis. Sci. Total Environ. 809, 151118 https://doi.org/10.1016/j.scitotenv.2021.151118.

Wise Jr., J.P., Young, J.L., Cai, J., Cai, L., 2022. Current understanding of hexavalent chromium [Cr(VI)] neurotoxicity and new perspectives. Environ. Int. 158, 106877 https://doi.org/10.1016/j.envint.2021.106877.

Zhang, L., Li, N., Zhang, X., Wu, H., Yu, S., 2023a. Hexavalent chromium caused DNA damage repair and apoptosis via the PI3K/AKT/FOXO1 pathway triggered by oxidative stress in the lung of rat. Ecotoxicol. Environ. Saf. 267, 115622 https://doi.org/10.1016/j.ecoenv.2023.115622.

Zhang, T., Feng, L., Cui, J., Tong, W., Zhao, H., Wu, T., Zhang, P., Wang, X., Gao, Y., Su, J., Fu, X., 2023b. Hexavalent chromium induces neurotoxicity by triggering mitochondrial dysfunction and ROS-mediated signals. Neurochem. Res. https://doi.org/10.1007/s11064-023-04063-y.